DOUBLE DIFFERENTIAL CONTINUUM NEUTRON SCATTERING CROSS SECTIONS IN IRON AND NICKEL FOR INCIDENT ENERGIES OF 7.5, 10 AND 12 MEV

by

ALBERT GEORGE BEYERLE, JR.

A thesis submitted to the Graduate Faculty of
North Carolina State University at Raleigh
in partial fulfillment of the
requirements for the Degree of
Doctor of Philosophy

DEPARTMENT OF PHYSICS

RALEIGH

1 9 8 1

APPROVED BY:

C. R. Gould Stephen R Cotanch

L. W. Seagondollar
Advisory Committee
Chairman

BIOGRAPHY

Albert George Beyerle, Jr. was born in Baltimore, Maryland on August 14, 1953. He was raised in Baltimore County and later near Annapolis, Maryland where he graduated from Annapolis Senior High School in June 1971.

The author entered North Carolina State University and received a Bachelor of Science degree in physics in May of 1975. He entered graduate school in physics at North Carolina State University, accepting a teaching assistantship, and later a research assistantship to pursue the research described herein.

The author has been married to the former Maren Oline Schmidt since December 1974. Maren Beyerle received a Bachelor of Science degree in Psychology from the University of North Carolina at Chapel Hill in May 1978.

TABLE OF CONTENTS

Page

LIST OF SYMBOLS v

I Introduction 1

II Experimental Procedure 5

2.1 Physical Apparatus 5

2.2 Electronics 22

III Data Reduction 33

3.1 Data Acquisition Program 33

3.2 Experimental Procedure 34

3.3 Offline Procedures 45

3.4 Normalization 52

IV Data Correction 54

4.1 Need for Data Correction 54

4.2 Approach to the Problem 59

4.3 Features of EFFIGYC 61

4.4 Method 65

4.5 Solution of the Multiple Scattering Problem . . 68

4.6 Iteration of Cross Section 72

V Analysis and Results 79

5.1 The Energy Distribution 79

5.2 Decay of the Compound System 81

5.3 Presentation of the Data 88

5.4 Discussion of the Uncertainties 110

5.5 Conclusion 114

Appendix A Multiple Scattering Rate Derivation 117

Appendix B Experimental Data 123

B.1 Iron at 7.5 MeV 123

B.2 Iron at 10 MeV 125

B.3 Iron at 12 MeV 127

B.4 Nickel at 7.5 MeV 129

B.5 Nickel at 10 MeV 131

B.6 Nickel at 12 MeV 133

LIST OF REFERENCES 135

SYMBOLS

B_b^a = Integrated beam current collected on the beam stop used for normalization purposes. The superscript "a" indicates the gas situation (in or out) and the subscript "b" indicates sample position. Further discussion of the meanings of sample in/out and gas in/out can be found in Chapter III.

BIAS = Number added to each channel each time a difference is taken to ensure that no negative values are obtained (usually BIAS=100).

C = Undefined constant.

C_b^a = Experimental counts with superscript "a" noting the gas situation and subscript "b" indicates sample situation.

${}_Z^A C$ = Compound nucleus with A nucleons and Z protons.

E_c = Compound nucleus excitation energy formed by the capture of a neutron by the target nucleus.

E_r = Energy of the residual nucleus after decay of the compound system by the emission of a neutron.

E_n = Energy of the incident neutrons in these experiments.

ΔE = Energy difference between the ground states of the target or residual nucleus and the compound nucleus.

ε, E_{out} = In Chapter V, ε is the energy of the emitted

neutrons which is equal to E_{out}.

E_i = Energy incident to the i^{th} order process.

E_a = Energy of a neutron as detected from the material denoted by subscript a. The value of a is "s" for the scattering sample or "poly" for the polyethylene normalization sample.

F = Functional describing the scattering process.

F^{-1} = Inverse of F

$f(x)$ = Function describing scattering process such that $\int_x f(x)\,dx = F$

F_{ab} = relative flux from source point a to sample point b.

g = The number of spin states for the neutron (=2).

h = Planck's constant divided by 2π.

L_b^a = Detection system live time to clock time ratio. This serves as a correction for system dead time.

m_n = Mass of a neutron.

n_a = Number of atoms in the sample denoted by subscript a. Meaning of a is defined with the symbol E_a.

N = number of test points chosen in Monte Carlo evaluation of an integral.

N_a = Count rate in the sample, denoted by the subscript a, defined as the number of counts in the experiment divided by the experimental integrated beam current. This is in fact the

experimental difference as defined in equation 3.1.

P_c = Production of neutrons in the solid material of the gas cell itself.

$P_d(\varepsilon)$ = Probability of decay of the compound system as a function of emitted neutron energy. This defines the shape of the energy spectra.

P_g = Production of neutrons in the gas contained within the cell.

r_{ab} = Distance between points a and b.

$\bar{r}_{ab}$ = Vector from point a to point b.

$\bar{r}^{i}_{ab}$ = Same as $\bar{r}_{ab}$ except superscript i denotes that this a vector associated with the i^{th} discrete test point.

$\bar{r}_a$ = Vector from origin to point a.

r_o = Radius of a single nucleon.

R = Total rate of scattering from all order processes.

$^{A}_{Z}R$ = Residual nucleus with A nucleons and Z protons.

R_i = Rate of scattering from ith order process.

$R_c(\varepsilon)$ = Rate of compound nucleus formation from the excited residual nucleus. This is not an observed process but a conceptual device.

$R_d(\varepsilon)$ = Rate of compound nucleus decay to the excited residual system.

R_p = Pearson linear correlation coefficient.

S_c = Defined as the logarithm (base e) of the compound system level density ($S_c = \ln(\rho_c)$).

S_r = Defined as the logarithm (base e) of the residual system level density ($S_r = \ln(\rho_r)$).

S_s = Scattering of neutrons from the sample.

S_x = Scattering of neutrons from things surrounding the sample but excluding the sample itself.

$S(t;E)$ = Beam resolution function. This includes both time and energy dispersion.

T = Nuclear temperature parameter.

$^{A}_{Z}T$ = Target nucleus with A nucleons and Z protons.

T_{ab} = transmission from source point a to sample point b.

T_{in} = Transmission probability for a neutron into the target nucleus.

v = Velocity

V = Volume

V_i = Volume of integration for the ith order scattering process used in the evaluation of the scattering rates.

V_{samp} = Volume of the scattering sample.

x = Multiplication operation.

η = Detector efficiency

Δ = Difference between the observed cross section (σ_{obs}) and the simulation based on the estimated cross section (σ_{est}).

Ω = Solid angle in steradians.

ρ_c = Level density of the compound system.

ρ_d = Level density available to the decay of the compound system which is the density of states available to the residual nucleus plus neutron.

ρ_r = Level density in the residual system.

σ = Cross section

σ_s^{bu} = Source breakup cross section.

σ_{est} = Estimate of continuum scattering cross section, based on the results of previous simulation.

σ_c = Cross section for the capture of a neutron by the target or residual nucleus.

σ^i = Cross section of i^{th} process. For example elastic, or inelastic scattering.

σ_i = Cross section of the i^{th} order process. For example, single or double scattering.

σ_{new} = New guess for estimated cross section for update of σ_{est}.

σ_{obs} = Observed cross section. This is the uncorrected experimental result which is to be put into EFFIGYC for correction.

σ_s = Source cross section.

σ_{total} = Total cross section for all types of interactions.

$\langle\ \rangle$ = Average of the enclosed quantity.

I Introduction

Neutron double differential scattering cross sections ($d^2\sigma/d\Omega dE_{out}$) exciting unresolvable high-lying levels in natural-abundance elemental iron and nickel nuclei have been measured for incident neutron energies between 7.5 and 12 MeV. Energy distributions for outgoing neutron energies above 0.5 MeV and up to about 2 MeV below the incident energy have been measured. These are referred to as "continuum" scattering measurements since we can not resolve the individual levels of the residual nuclei in these experiments due to the large number of closely spaced levels and we must deal with the collective properties of many such levels. Some of this work has been previously reported[1,2]. Our experiment and results are described here in detail.

This experiment fits in with the TUNL program of scattering measurements. Discrete scattering studies to low-lying resolvable levels have been previously carried out at TUNL by Hogue[3] and Glendinning[4] and are still being carried out for medium mass nuclei by El-Kadi[5]. The continuum measurements represent a new phase for the TUNL neutron scattering program.

The idea of continuum scattering is not new. These measurements have been made in the incident neutron energy range below 7.5 MeV for example by Towle and Owen[6], Thomson[7], Wilenzick[8], and Kinney[9] and at around 14 MeV, for example by Stengl et. al.[10] and Mather et. al[11]. Experimental difficulties have prevented the filling of the area between 7.5 and 12 MeV. Only recently has this gap begun to close due to measurements such as ours and for example those by Drake et. al.[12] or Biryukov et. al.[13] In principle, the measurements of the angular and energy distributions are not difficult. If neutrons of the desired energy strike a sample of scattering material from a known direction, then detectors placed at various angles with respect to the incident neutrons can be used to measure the angular and energy distributions of the scattered neutrons and thereby arrive at scattering cross sections. Unfortunately this ideal experiment can not be carried out. Properties of neutrons and their interactions with matter introduce many complications that are difficult to account for. Paramount among these are neutron production and detection difficulties.

Neutrons produced by material other than the desired source and undesirable neutrons from even the best sources are complicating factors. In fact, the lack of a monoenergetic neutron source is the principal reason for the

lack of data in this energy range. The fact that there is no neutron detector for these neutrons which will give direct energy information, as there is for charged particles or electromagnetic radiation, requires that time-of-flight techniques must be used for energy spectroscopy. Detection efficiencies which depend on neutron energy and response of the detection material to gamma rays also complicate neutron detection. In addition, large scattering samples and scattering materials other than the sample material in the vicinity of the sample (air for example) add further complications. In as much as is possible, these complicating factors have been accounted for experimentally. This is accomplished by careful experimental design and experimental isolation and measurement of as many of the undesirable effects as possible. However, some of the effects must be removed by calculation. As will be discussed, the calculation of the neutron source complications are one of the most unique features of these measurements. These calculations are carried out by the computer program EFFIGYC.

The motivation for these measurements is two-fold. Iron and nickel are important structural materials for fusion reactor design and cross section data are necessary for all energies below 14 MeV (the energy carried away by the neutron in a low energy $T(d,n)^4He$ reaction). These data

also provide level density information on nuclei and serve to bridge the 7.5 to 14 MeV gap in data where other channels ((n,2n), (n,np)) begin to open up and may effect the results.

II Experimental Procedure

2.1 Physical Apparatus

In order to carry out neutron scattering measurements, neutrons are produced by source reactions involving high velocity charged particles. To produce these charged particle beams, the TUNL direct extraction negative ion source (DENIS II) is used. This source delivered about 85 μA of negative hydrogen ions of which about 1 μA was delivered on the charged particle target. The ion beam is passed through a radio-frequency 'chopper' which subjects the beam to a transverse electric field that is varying sinusoidally with time at a frequency of 2 MHz. The resulting transverse displacement, sweeps the beam across a 0.375 inch aperture located in the beam tube. This produces a beam pulse every 250 nsec. An auxiliary chopper removes all but every fourth pulse by application of a transverse electric field square-wave tuned to sweep the pulses out of the acceptance of the beam optics system. This yields pulses every 1 micro-second. These pulses are 'bunched' by application of a longitudinal electric field, sinusoidally varying in time, which decelerates the leading part of the pulse and accelerates the trailing part to compress or bunch

the beam into a very narrow pulse. Typical beam pulse widths on target are about 2 nsec full width at half maximum.

Beam pulses are accelerated, charge changed, and further accelerated by the TUNL tandem Van de Graaff accelerator. The positively charged particle beam so produced is transported to the target via the 38^{o} beam line to the neutron time-of-flight scattering area. Details of the TUNL ion sources, accelerator, and beam transport systems have been previously described[14,3,4,15].

For reasons to be discussed later, some of these experiments require the use of tritium gas which is radioactive. The use of the relatively large amounts of radioactive gas contained by a gas cell and a thin foil requires careful measures to minimize radiation hazards to the environment. The tritium safety system has been discussed in detail by Purser[16] and briefly by Seagondollar[15].

Neutrons are produced, by charged particle bombardment of appropriate nuclei, in a gas volume contained at the end of the beam line in a gas cell (the accelerator target). In this work two gas cells were used. The first cell has been discussed elsewhere[3]. This cell contains deuterium gas, and

is made of thin-walled stainless steel, as illustrated in figure 2.1. The inside of the cell is lined with a removable tantalum liner and has a tantalum beam stop to reduce neutron backgrounds from the cell materials. The cell is sealed from the beam line and outside atmosphere with an indium "O" ring. It is pressurized to 30 psia with high purity deuterium which has been passed through a liquid nitrogen trap before entering the cell to remove hydrocarbon contaminates. This cell is used to produce neutrons via the $D(d,n)^3He$ reaction.

The second cell is used exclusively for tritium gas to minimize contamination of the tritium system with other hydrogen isotopes. It is illustrated in figure 2.2. The cell[15] is constructed of thin walled stainless steel and contains a tantalum liner. Neutrons are produced in this cell by the $T(p,n)^3He$ reaction. Since the protons impinging on the cell walls at the proton energies needed copiously produce neutrons, the choice of those cell materials which are struck by the protons is particularly important. Studies of this matter have been carried out by Drosg, et. al.[17] with the conclusion that Ni^{58} is the best material for the beam stop. A Ni^{58} beam stop is used in this cell. The entrance foil, which is molybdenum, is cemented in place with epoxy glue as a seal from the beam line vacuum. Molybdenum entrance foils are used rather than ^{58}Ni due to

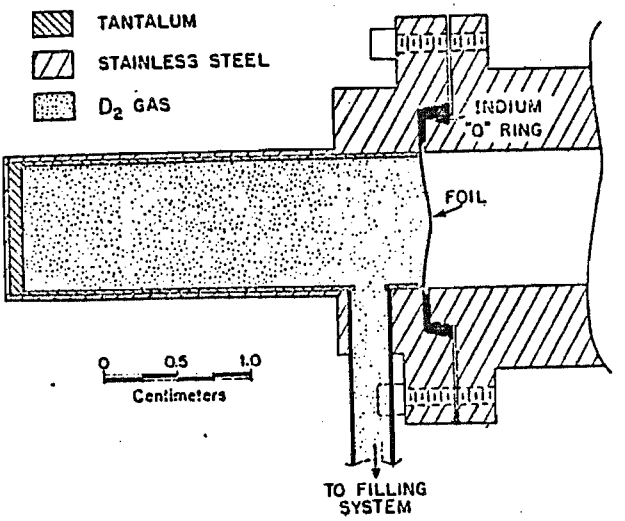

Figure 2.1 Deuterium gas cell

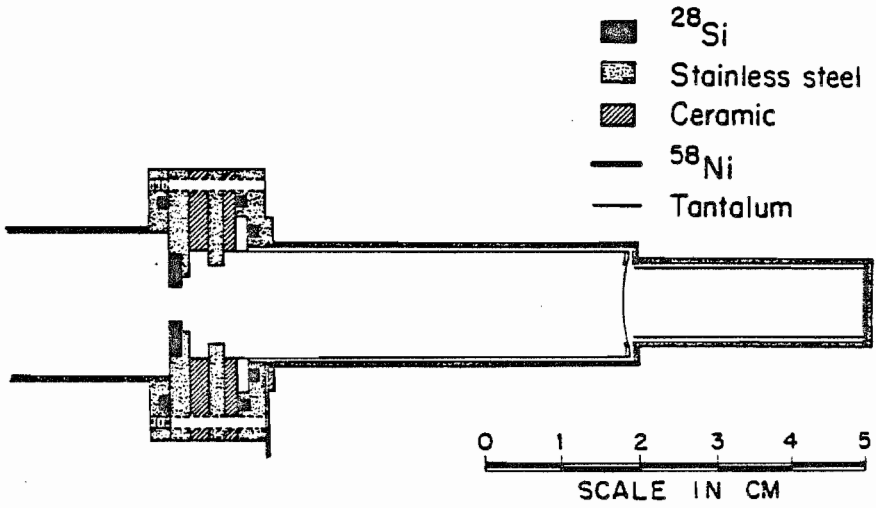

Figure 2.2 Tritium gas cell

difficulties with the quality of the Ni foils and the greater relative danger of a foil rupture. The tritium is prevented from escaping to the outside environment by two "viton" "O" rings. Before the cell is pressurized with T_2, it is tested statically with 3 atmospheres (45 psia) of He gas for foil leaks and then for at least 30 minutes with twice the beam used in the data taking run. Then the cell is filled with tritium gas which is stored in a uranium furnace. (Tritium is stored in the form of UT_3 in a furnace of sintered uranium powder. The tritium is liberated by the heating of the furnace and can be recaptured by allowing it to enter the cool furnace. Other gasses, particularly the reaction by-products, are easily removed since the tritium storage system will store only hydrogen. At present the tritium contains about 10-15% H_2 and an insignificant amount of D_2 gas.)

The choice of the neutron source reaction is critical for these measurements. To avoid extremely difficult problems in data analysis, it is highly desirable to do these experiments with monoenergetic neutrons. Unfortunately all neutron producing reactions in the energy range of this work produce some neutrons of energy lower than that of the primary neutron group. The lower energy neutrons from our sources must be minimized as they cannot be accounted for experimentally. (Experimental efforts to account for other

lower energy neutrons produced by things other than the source gas will be discussed in Chapter III.) The most nearly monoenergetic source reactions are those involving isotopes of hydrogen. Reactions involving heavier elements all may lead to bound excited states in the residual nucleus and thus lead to more than one discrete neutron group. For these measurements, the $D(d,n)^3He$ and the $T(p,n)^3He$ reactions are used as they produce the most nearly monoenergetic neutrons in the correct energy range. These source reactions have been studied extensively at Los Alamos Scientific Laboratory[18] and at TUNL[19] for this energy range.

The D(d,n) reaction has been used for the 7.5 MeV neutron energy data. The threshold for deuteron breakup (D(d,p+n)D) corresponds to about 7.5 MeV neutron energy. The deuterons can breakup on the heavier elements of the cell itself at these energies but these breakup effects can be accounted for experimentally. Therefore the breakup of the source gas deuterons is not a problem at this energy. The D(d,n) reaction has the advantage that its cross section is higher and the angular distribution of the neutrons is more forward peaked. This results in a neutron flux at our scattering sample that is about a factor of three higher than that of our other choice, the T(p,n) reaction. The more forward-peaked angular distribution also reduces the room-scattered background by producing relatively fewer

neutrons which do not scatter off of the sample. An example of a D(d,n) time-of-flight source spectrum is shown in figure 2.3.

The $T(p,n)^3He$ reaction is used for the higher incident neutron energies of 10 and 12 MeV. As shown in figure 2.4, the ratio of production cross section for source gas breakup neutrons to that of the primary neutrons rises faster in the D(d,n) source[18]. We feel that the lower neutron production cross sections and higher isotropy of the T(p,n) source is offset by the fact that the experimentally unsubtractable gas breakup background is substantially less for this reaction. It should be pointed out that the T(p,n) reaction is not much better than the D(d,n) reaction if all undesired neutrons are taken into account. The T(p,n) reaction produces many neutrons from the gas container and also many gamma rays. These backgrounds, though large, are experimentally subtractable. A typical $T(p,n)^3He$ 0° source time-of-flight spectrum is shown in figure 2.5. It was obtained with one of the main detectors at 0° with no scattering sample in place.

Scattering samples used in this work are of natural elemental material. All samples are cylindrical and are mounted on a wire co-axial with the pivot axis of the detectors. The geometry is shown in figure 2.6. Samples

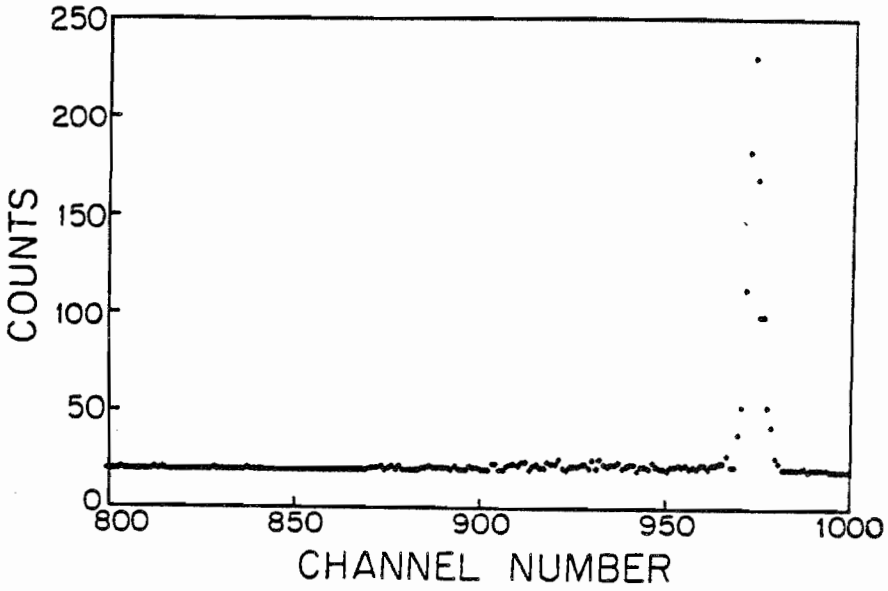

Figure 2.3 Neutron energy distributions from the $D(d,n)^3He$ source reaction at 0° for primary neutron energy of 7.5 MeV. Note that there are no gas-breakup neutrons.

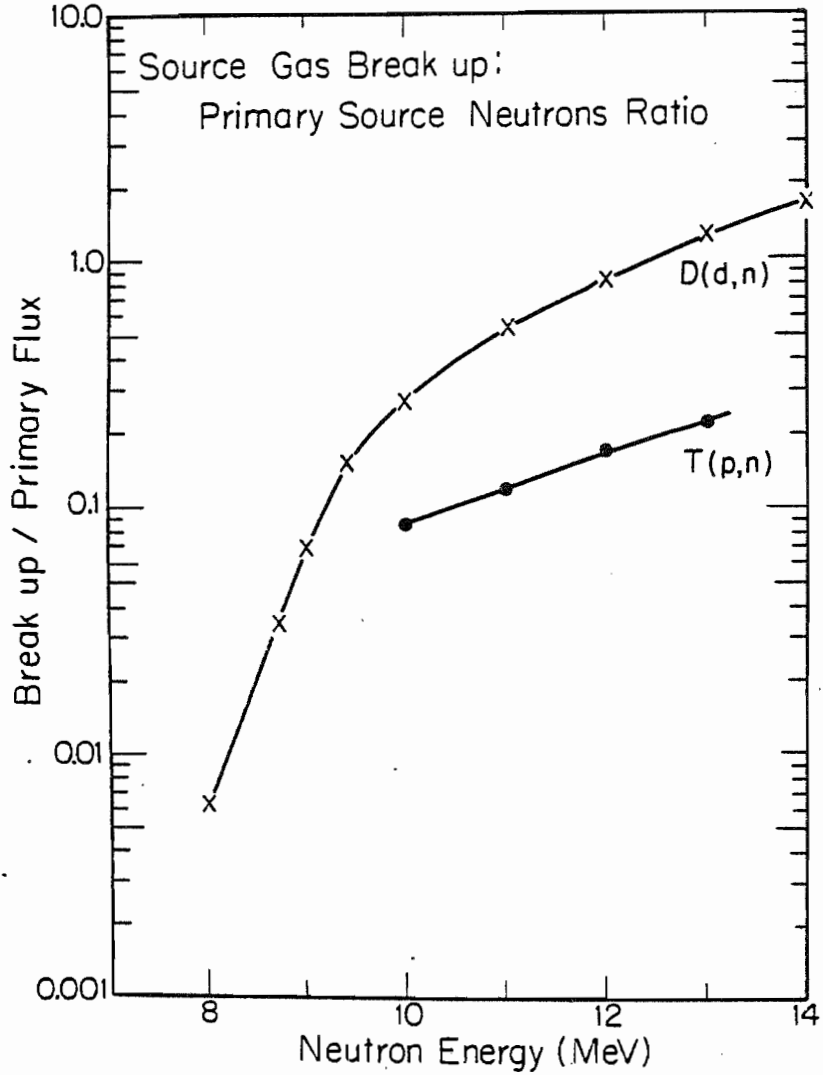

Figure 2.4 Ratio of gas breakup neutrons to primary source neutrons as a function of primary neutron energy. This is the component if the noise-to-signal ratio which cannot be accounted for experimentally.

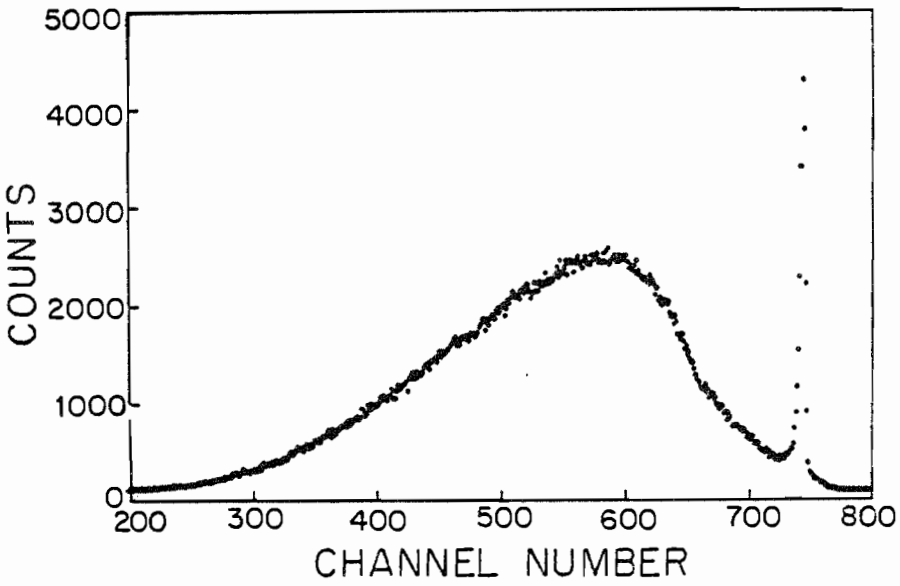

Figure 2.5 Typical $T(p,n)^3He$ 0^o source neutron energy distribution at 12 MeV primary neutron energy. Note that the source is not monoenergetic with the low energy component primarily due to neutron produced in the cell walls.

have a 3 centimeter outside diameter, are hollow with a 1.3 centimeter diameter hole along the sample symmetry axis, and are 4.4 centimeters in height. The nickel sample has a mass of 230.5 grams and the iron cylinder has a mass of 202.7 grams. The wire is hung over precisely located pulleys on the ceiling and just over the detector goniometer table. Tension is kept in the upper pulley with a weight attached to the upper end of the wire. The wire may be moved up and down with a stepping motor with up to four samples located along the wire. This allows positioning of scattering samples remotely. A Zeiss optical level is used to check of the proper centering the samples. The samples may also be computer driven allowing the automatic positioning of the samples by entering the sample desired. This system allows positioning of the sample to within 1/80 inch.

Neutrons are detected with massively shielded NE213 liquid scintillators. Time-of-flight techniques (TOF) are used to determine the energy of scattered neutrons. The main detectors are located on carriages which allow radial positioning of the scintillators from 2.5 to 3.9 meters for the "4-meter" detector and 2.5 to 5.7 meters for the "6-meter" detector. For the present experiments, the detector distances are set at 2.76 and 3.76-meters for the "4-meter" and "6-meter" respectively. All liquid scintillators are 2 inches in depth. The main scintillators

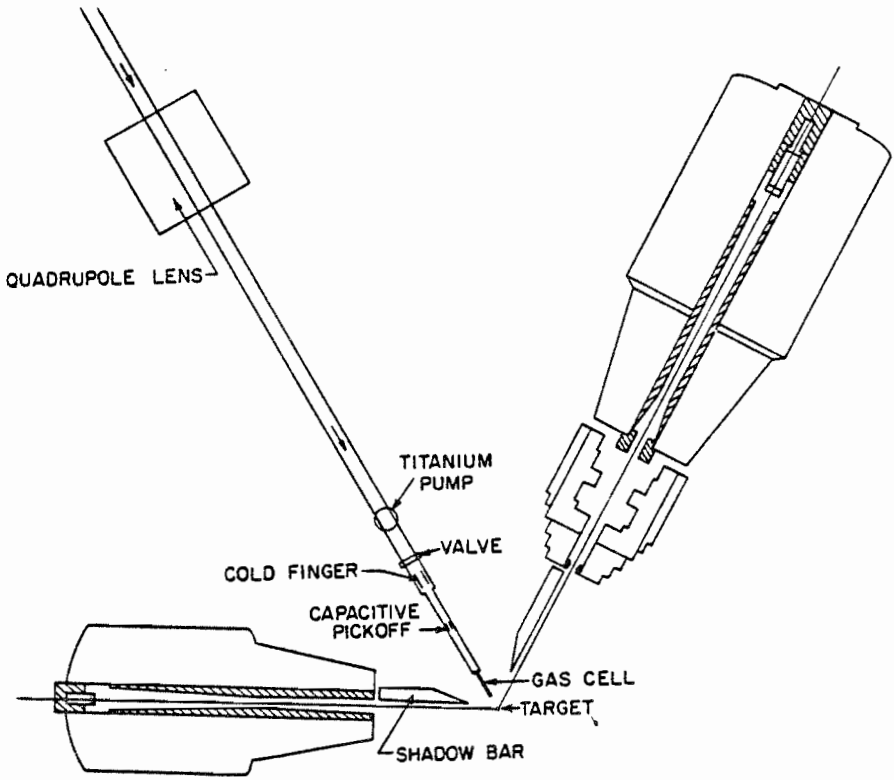

Figure 2.6 Scattering geometry. Shows location of detectors, shadow bars, scattering sample (or target), gas cell, and various beam line components.

are 3.5 inches and 5 inches in diameter for the "4-meter" and "6-meter" detectors respectively. The continuum flight paths are chosen to allow slow neutrons from a given burst to arrive at the "6-meter" detector before the fastest neutrons from the next beam burst can catch up with them and the "4-meter" is placed to achieve approximately the same count rate as the "6-meter".

The "6-meter" detector shield assembly is shown in cross section in figure 2.7, and the "4-meter" shield, while a bit shorter in axial length, is very similar (see Hogue [3] and Glendinning [4]). The shields weigh about 5000Kg and contain primarily a mixture of paraffin and lithium carbonate as described by Glasgow[20]. The throat of the detector contains a doubly-truncated conical collimator to reduce in-scattering effects. The collimator is designed so that a neutron that scatters from the front quarter of the collimator cannot reach the detector without passing through additional collimator material as it will be screened by that part of the collimator closer to the detector. The back three-fourths of the collimator is designed so that neutrons entering the front of the detector cannot strike this portion of the collimator directly. Also the collimator must not screen any of the sample from any of the detector yet shield as much of the detector as possible from neutrons other than those which scatter from the sample. In

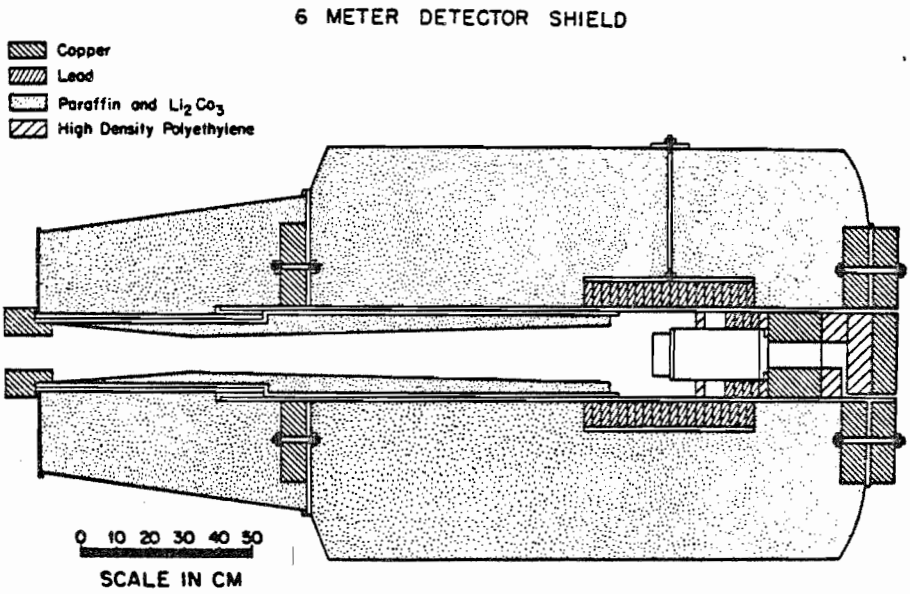

Figure 2.7 Cross section view of the "6-meter" neutron detector and its shield.

this manner the collimator allows no neutron to scatter from the collimator and still reach the detector without either passing through additional collimator material or scattering more than once. A detailed analysis of such doubly-truncated collimators was made by Glasgow[20]. Behind the scintillator is copper and high-density polyethylene in the "6-meter" and paraffin and copper in the "4-meter" detector. More paraffin behind the "4-meter" detector is added at the beginning of each run to provide additional shielding. This is made necessary for the low-bias measurements because fast neutrons may scatter from the walls of the target area and reach the detector at the same time as slower, low energy neutrons directly from the scattering sample.

The massive detector shield assemblies are mounted on carriages which pivot about the scattering sample axis. Detector angles are measured by verniers located on the goniometer. To enable movement of these shields, each carriage is driven by an electric motor mounted on the rear of the carriages and controlled near the pivot axis.

In addition to the main detectors, there are two monitor detectors. A flux monitor is located about two meters from the gas cell, mounted on the ceiling at a neutron production angle relative to the beam axis of 90 degrees. This